EARTHQUAKE ENGINEERING AND STRUCTURAL DYNAMICS, VOL. 26, 441–462 (1997)

DAMAGE MODELS FOR THE SEISMIC RESPONSE OF BRICK MASONRY SHEAR WALLS. PART II: THE CONTINUUM MODEL AND ITS APPLICATIONS

L. GAMBAROTTA AND S. LAGOMARSINO

Department of Structural and Geotechnical Engineering, University of Genoa, via Montallegro 1, 16145 Genoa, Italy

SUMMARY

The damage model for mortar joints proposed in the companion paper (Reference 1) is here applied to an extended approach for the evaluation of the lateral response of in-plane loaded brick masonry shear walls. The continuum model considered here is based on the simplifying assumption of an equivalent stratified medium made up of layers representative of the mortar bed joints and of the brick units and head joints, respectively. The constitutive equations for the brick masonry are obtained through a homogenization procedure involving the damage model proposed in the companion paper and simple damage constitutive equations for the brick layer. The constitutive model is used in a finite element analysis of the lateral response of brick masonry shear walls in-plane loaded either by cyclic horizontal actions superimposed on vertical loads or by dynamic loads, which are representative of the seismic actions. The capabilities and the validity limits of the finite element analysis obtained by the continuum approach are indicated from the simulation of experimental results concerning rectangular slender and squat shear walls and also by the comparison with the theoretical results from the composite model proposed in the companion paper. Moreover, simulations of the experimental results from large-scale brick masonry shear walls carried out at the University of Pavia are presented. Finally the same shear wall has been analysed under dynamic strong motion at the base from which the suitability of the approach for the evaluation of the seismic vulnerability of masonry buildings emerges. © 1997 by John Wiley & Sons, Ltd.

KEY WORDS: masonry walls; constitutive equations; damage; continuum model; finite element analysis; dynamic response

1. INTRODUCTION

In evaluating the seismic vulnerability of masonry buildings, a fundamental task concerns the prevision of the in-plane response of the shear walls, which, because of their large scale and complex shape, may be arduous. Although several models for the analysis of brick masonry walls have been proposed, as discussed in the companion paper (Reference 1), when large-scale shear walls have to be analysed, a finite element modelling of the two-dimensional domain is needed together with constitutive equations based on a continuum representation of the masonry.

To this end constitutive equations have been proposed and they are based either on the smeared crack approach[2] or on the assumption of a no tensile strength continuum,[3] both allowing the evaluation of the lateral strength of the shear wall. Nevertheless, if more detailed knowledge is required concerning the post-critical and hysteretic response, it follows that it is very important to take into account the masonry inhomogeneity and the damage of single materials. Recently, constitutive models based on the homogenization of the masonry have been formulated through different approaches,[4–7] some of them concerning the elastic characterization of the brick masonry.[8,9] However, these models do not seem to have been applied to the two-dimensional analysis of shear walls.

In this paper, a continuum damage model for brick masonry is formulated and applied to the analysis of large shear walls. It is based on the mortar joint model presented in the companion paper,[1] and is capable of taking into account both the tensile versus compressive response of mortar joints and the hysteretic response

CCC 0098–8847/97/040441–22$17·50

Received 5 March 1996
Revised 11 October 1996

to cyclic shearing strains. The constitutive equations (Section 2) proposed here allow the behaviour of the masonry components to be taken into account by means of a homogenization process of a layered medium assumed representative of the brick masonry. This simplified approach considers two typical layers: the mortar bed joint layer and the layer representative of the brick and mortar head joints; the former is modelled in order to take into account decohesion and slippage in the interface, while the latter considers the damage and failure of bricks. The inelastic strains in mortar joints and bricks are postulated according to damage mechanics and take into account the frictional sliding in the mortar joint interfaces. Moreover, the simplifying assumptions of ignoring the contributions to the strain due to the presence of the mortar head joints and to the weakening effects of the horizontal stresses are put forward.

The constitutive equations proposed here are used in a finite element analysis of two-dimensional shear walls by means of an incremental-iterative analysis which has been subsequently extended in a general-purpose finite element code (Section 3). To this end an *ad hoc* procedure for the integration of the constitutive equation in the finite load step has been developed based on a description involving three internal variables which evolve during the incremental analysis. Even if the proposed model is characterized by several parameters, it is shown that they may be evaluated directly by tests on materials and on simple assemblages of units.

The experimental results obtained by Anthoine *et al.*[10] for two rectangular walls already considered in the companion paper[1] have been simulated by the proposed model (Section 4). The analysis concerns both a squat and a slender wall in order to give an interpretation of the different hysteretic response exhibited by the two walls in terms of the proposed model. To show the capabilities of the finite element model to analyse large-scale shear walls, the simulation of the response of the shear wall experimented by Calvi and Magenes[11] has been carried out. In this case the model has shown good suitability in describing the hysteretic response, the damage mechanisms in the mortar joints and in evaluating the lateral strength. Finally, the same shear wall has been analysed with reference to a prescribed horizontal load history described by a proper base accelerogram; the effects induced on the wall, such as lateral stiffness degradation and mortar joint and brick damage, turn out to be similar to those observed under quasi-static loads. The reliability of the continuum model here proposed and applied and its validity limits are pointed out by the discussion of the results given by the simulations and examples.

2. CONTINUUM DAMAGE MODEL FOR BRICK MASONRY

The constitutive equations for in-plane loaded brick masonry are obtained on the hypothesis of plane stress condition and by considering the brick masonry as a stratified medium made up of two typical layers: the bed mortar joint layer and the layer representative of the mortar head joints and the brick units. This approximation, which is analogous to those put forward by Pietruszczac,[4] Pietruszczac and Niu[5] and Pande *et al.*,[8] only considers the inelastic strains in the mortar bed joint and in brick units, so ignoring the mechanisms of inelastic deformation involving the head joints together with the bed joints, already described in the companion paper.[1]

The constitutive equations regarding the equivalent continuum damage model are then obtained by homogenizing the stratified medium. This is carried out by considering a representative volume element[12] having unit width and height $b + s$ (s and b are, respectively, the joint and brick unit heights) and by defining the mean stress $\boldsymbol{\sigma} = \{\sigma_1, \sigma_2, \gamma\}^t$ and strain $\boldsymbol{\varepsilon} = \{\varepsilon_1, \varepsilon_2, \gamma\}^t$ (ε_2 is the normal strain in the direction normal to the mortar bed joints). The mean strain may be expressed as follows:

$$\boldsymbol{\varepsilon} = \mathbf{K}_M \boldsymbol{\sigma} + \eta_m \boldsymbol{\varepsilon}_m^* + \eta_b \boldsymbol{\varepsilon}_b^* \tag{1}$$

where $\boldsymbol{\varepsilon}_m^* = \{0, \varepsilon_m, \gamma_m\}^t$ and $\boldsymbol{\varepsilon}_b^* = \{0, \varepsilon_b, \gamma_b\}^t$ are the inelastic strains in mortar joint and bricks respectively, $\mathbf{K}_M$ is the elastic orthotropic compliance matrix of the masonry and $\eta_m = s/(b + s)$ and $\eta_b = 1 - \eta_m$ are the volume fraction of the mortar and of the brick respectively.

The matrix $\mathbf{K}_M$ has the form:

$$\mathbf{K}_M = \begin{bmatrix} \dfrac{1}{E_{M1}} & -\dfrac{\nu_{M12}}{E_{M1}} & 0 \\ -\dfrac{\nu_{M12}}{E_{M1}} & \dfrac{1}{E_{M2}} & 0 \\ 0 & 0 & \dfrac{1}{G_M} \end{bmatrix} \tag{2}$$

in which the moduli E_{M1}, E_{M2}, ν_{M12} and G_M depend on the elastic moduli of mortar (E_m, ν_m) and brick (E_b,ν_b) and on parameters characterizing the geometry of the masonry pattern and may be obtained on the basis of homogenization techniques such as those proposed by several authors.[7–9] In particular, these moduli may be approximated simply by ignoring the head mortar joints as follows:

$$E_{M1} = \eta_m E_m + \eta_b E_b \tag{3}$$

$$E_{M2} = \left[\frac{\eta_b}{E_b} + \frac{\eta_m}{E_m} - \frac{\eta_m \eta_b E_m E_b}{E_{M1}} \left(\frac{\nu_b}{E_b} - \frac{\nu_m}{E_m} \right)^2 \right]^{-1} \tag{4}$$

$$\nu_{M12} = \eta_m \nu_m + \eta_b \nu_b \tag{5}$$

$$G_M = \left(\frac{\eta_m}{G_m} + \frac{\eta_b}{G_b} \right)^{-1} \tag{6}$$

where only the parameters representing the masonry geometry are the volume fractions. The diagrams of Figure 1 show the sensitivity of the overall moduli E_{M2} and G_M on the brick volume fraction given from equations (4) and (6).

The mechanism of inelasticity in the bed mortar joint is expressed on the basis of the mortar joint model proposed in the companion paper[1] and concerns the extension ε_m and the sliding γ_m, assumed linearly dependent on the applied stress as follows:

$$\varepsilon_m = c_{mn} \alpha_m H(\sigma_2) \sigma_2 \tag{7a}$$

$$\gamma_m = c_{mt} \alpha_m (\tau - f) \tag{7b}$$

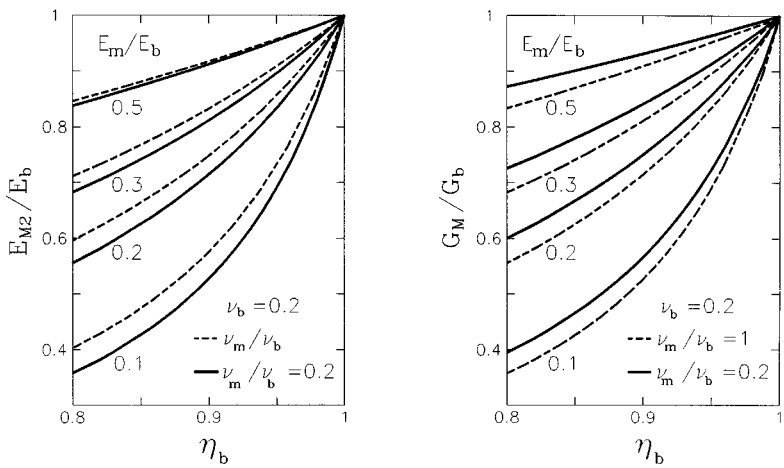

Figure 1. Overall elastic moduli of the masonry from equations (4) and (6) as a function of the brick volume fraction η_b and of the elastic moduli of the single components

here σ_2 and τ are the resolved stresses on the mortar bed joint, α_m ($\geqslant 0$) is the mortar joint damage variable, H is the Heaviside function taking into account the unilateral response of the interface and c_{mn} and c_{mt} are the extensional and tangential inelastic compliance parameters characterizing the bed mortar joint. Finally, f is representative of the friction in the mortar–brick interface;[1] when tensile stress ($\sigma_2 \geqslant 0$) acts on the mortar joint the variable f vanishes, while under compressive stresses ($\sigma_2 < 0$) it limits or locks the sliding induced by the shear stress.

The mechanism of inelasticity of brick damage is simply described by taking into account the effects of the vertical compressive and shear stresses on the corresponding inelastic strain components which are assumed, analogous to the mortar joint, as follows:

$$\varepsilon_b = c_{bn}\alpha_b H(-\sigma_2)\sigma_2 \tag{8a}$$

$$\gamma_b = c_{bt}\alpha_b\tau \tag{8b}$$

where $\alpha_b(\geqslant 0)$ represents the damage in bricks, c_{bn} and c_{bt} are the compressive and tangential compliance parameters of the bricks. In equation (8a) the Heaviside function H takes into account only the vertical compressive strain in bricks; in fact, the inelastic vertical extension in the masonry is localized in the bed–mortar joint because of their low strength in comparison with the tensile strength of the bricks. Moreover, the contraction ε_b has to be intended as the overall effect of the brick and mortar damage due to compressive stress on the bed joint plane. These simple assumptions for the brick constitutive model may be supported by the consideration, corroborated by the examples analysed in detail by the composite model presented in the companion paper,[1] that the collapse mechanisms of shear masonry walls are first characterized by the failure in mortar bed joints and successively, after a wide inelastic phase, by the brick failure. Thus the constitutive assumptions ruled by equations (8) seem to be acceptable, the subject of this analysis being limited to brick masonry shear walls.

From equations (1), (7) and (8) one can evaluate the strain corresponding to a given stress once the internal variables α_m, γ_m and α_b are known. To this end, as the dissipation in the infinitesimal step, expressed according to Reference 13 is as follows:

$$D = \eta_m Y_m\dot{\alpha}_m + \eta_m f\dot{\gamma}_m + \eta_b Y_b\dot{\alpha}_b \tag{9}$$

the affine variables lead to the density of damage energy release rate in the mortar joint

$$Y_m = \tfrac{1}{2}c_{mn}H(\sigma_2)\sigma_2^2 + \tfrac{1}{2}c_{mt}(\tau - f)^2 \tag{10}$$

the friction f and the density of damage energy release rate in bricks

$$Y_b = \tfrac{1}{2}c_{bn}H(-\sigma_2)\sigma_2^2 + \tfrac{1}{2}c_{bt}\tau^2 \tag{11}$$

The evolution equations are formulated on the basis of three conditions which must be satisfied during the loading process; they are defined according to criteria already applied for the mortar joint model.[1] The damage evolution in mortar joints and bricks is defined by imposing the corresponding damage energy release rate to be less than or equal to proper toughness functions (assumed depending on the damage variables):

$$\phi_{dm} = Y_m - R_m(\alpha_m) \leqslant 0 \tag{12}$$

$$\phi_{db} = Y_b - R_b(\alpha_b) \leqslant 0 \tag{13}$$

In analogy with the joint model presented,[1] the joint and brick toughnesses R_m and R_b must satisfy the conditions

$$R(\alpha) \to 0 \quad \alpha \to 0 \tag{14a}$$

$$2R(\alpha) + \alpha R'(\alpha) > 0 \quad \forall\alpha > 0. \tag{14b}$$

Thus, when the limit condition $\phi_{dm} = 0$ ($\phi_{db} = 0$) is reached in the infinitesimal load step, the joint damage rate $\dot{\alpha}_m$ (brick damage rate $\dot{\alpha}_b$) is assumed to take place.

Moreover, when the mortar bed joints are compressed ($\sigma_2 < 0$), the variable f has to satisfy the friction limit condition

$$\phi_s = |f| + \mu\sigma_2 \leqslant 0 \tag{15}$$

involving the friction coefficient μ, to which the simple flow rule corresponds

$$\dot{\gamma}_m = v\dot{\lambda}, \quad \dot{\lambda} \geqslant 0 \tag{16}$$

with $v = f/|f|$.

Such an approach provides a different response according to the tensile or compressive stress acting on the mortar bed joint. To distinguish these two possibilities it may be pointed out that from equations (1), (2), (7) and (8) it follows that when tensile stress is acting ($\sigma_2 \geqslant 0$) it leads to $(1/E_{M2} - \nu_{M12}/E_{M1} + \eta_m c_{mn}\alpha_m)\sigma_2 = \nu_{M12}\varepsilon_1 + \varepsilon_2$, while under compressive stress ($\sigma_2 < 0$) it leads to $(1/E_{M2} - \nu_{M12}/E_{M1} + \eta_b c_{bn}\alpha_b)\sigma_2 = \nu_{M12}\varepsilon_1 + \varepsilon_2$. Thus, since the terms between brackets are positive because of the positive definiteness of the matrix $\mathbf{K}_M$ and of the inelastic compliances, it follows that $\mathrm{sgn}(\sigma_2) = \mathrm{sgn}(\nu_{M12}\varepsilon_1 + \varepsilon_2)$.

When the tensile stress acts on the bed mortar joints ($\sigma_2 \geqslant 0$) both the damage mechanisms in the joint and in the bricks may be active and conditions (12) and (13), respectively, become

$$\phi_{dm} = \tfrac{1}{2} c_{mn}\sigma_2^2 + \tfrac{1}{2} c_{mt}\tau^2 - R_m(\alpha_m) \leqslant 0 \tag{17}$$

and

$$\phi_{db} = \tfrac{1}{2} c_{bt}\tau^2 - R_b(\alpha_b) \leqslant 0 \tag{18}$$

If both mechanisms are active ($\phi_{dm} = \phi_{db} = 0$), the infinitesimal damage increments $\{\dot{\alpha}_m, \dot{\alpha}_b\}^t$ may be obtained as the solution of the linear complementary problem

$$\begin{Bmatrix} \dot{\phi}_{dm} \\ \dot{\phi}_{db} \end{Bmatrix} = -\begin{bmatrix} R'_m & 0 \\ 0 & R'_b \end{bmatrix} \begin{Bmatrix} \dot{\alpha}_m \\ \dot{\alpha}_b \end{Bmatrix} + \begin{Bmatrix} c_{mn}\sigma_2\dot{\sigma}_2 + c_{mt}\tau\dot{\tau} \\ c_{bt}\tau\dot{\tau} \end{Bmatrix} \leqslant \mathbf{0} \tag{19a}$$

$$\{\dot{\alpha}_m \quad \dot{\alpha}_b\}^t \geqslant \mathbf{0} \tag{19b}$$

$$\{\dot{\phi}_{dm} \quad \dot{\phi}_{db}\}\{\dot{\alpha}_m \quad \dot{\alpha}_b\}^t = \mathbf{0} \tag{19c}$$

The uniqueness of the solution is guaranteed if $R'_m > 0$ and $R'_b > 0$. On the contrary, if $R'_m < 0$ two solutions $\dot{\alpha}_{m1} = 1$ and $\dot{\alpha}_{m2} > 0$ are possible, related to the decrement $c_{mn}\sigma_2\dot{\sigma}_2 + c_{mt}\tau\dot{\tau} < 0$. Analogously, when $R'_b < 0$ two solutions $\dot{\alpha}_{b1} = 1$ and $\dot{\alpha}_{b2} > 0$ are possible, which correspond to $c_{bt}\tau\dot{\tau} < 0$. However, different increments of the inelastic strains correspond to this variety of solutions. By assuming toughness functions characterized by the maxima R_{mc} and R_{bc} attained for the damage level defined by $\alpha_m = 1$ and $\alpha_b = 1$, respectively, it is possible to obtain the failure limit state for the bed mortar joint and the brick layer when tensile stress is acting $\sigma_2 \geqslant 0$. By posing $\phi_{dm}(\alpha_m = 1) = 0$ and $\phi_{db}(\alpha_b = 1) = 0$ the limit state for the mortar joint and for the brick are, respectively, given by

$$\sigma_2^2 + \rho_m\tau^2 = 2R_{mc}/c_{mn} = \sigma_{mr}^2 = \rho_m\tau_{mr}^2 \tag{20}$$

and

$$\tau^2 = 2R_{bc}/c_{bt} = \tau_{br}^2 \tag{21}$$

where σ_{mr} and τ_{mr} are the tensile and shear strength of the mortar joint, τ_{br} is the shear strength of the bricks and $\rho_m = c_{mt}/c_{mn}$. As a result the limit domain of brick masonry in the plane ($\sigma_2 \geqslant 0, \tau$) is obtained by the inner envelope of equations (20) and (21).

If the bed mortar joints are subjected to compressive stress ($\sigma_2 < 0$), three different mechanisms may be activated in the brick masonry: sliding and damage in the bed joints and damage in the bricks. In this case conditions (12), (15) and (13), considering equation (7b), may be expressed in terms of the internal variables

and of the applied stresses as follows:

$$\phi_{\mathrm{dm}} = \frac{1}{2}\frac{\gamma_{\mathrm{m}}^2}{c_{\mathrm{mt}}\alpha_{\mathrm{m}}^2} - R_{\mathrm{m}}(\alpha_{\mathrm{m}}) \leqslant 0 \tag{22}$$

$$\phi_{\mathrm{s}} = \left|\tau - \frac{\gamma_{\mathrm{m}}}{c_{\mathrm{mt}}\alpha_{\mathrm{m}}}\right| + \mu\sigma_2 \leqslant 0 \tag{23}$$

$$\phi_{\mathrm{db}} = \tfrac{1}{2}c_{\mathrm{bn}}\sigma_2^2 + \tfrac{1}{2}c_{\mathrm{bt}}\tau^2 - R_{\mathrm{b}}(\alpha_{\mathrm{b}}) \leqslant 0 \tag{24}$$

If the conditions (22)–(24) are satisfied at the limit state ($\phi_{\mathrm{dm}} = \phi_{\mathrm{s}} = \phi_{\mathrm{db}} = 0$) the infinitesimal increments of the internal variables $\dot{\alpha}_{\mathrm{m}}$, $\dot{\gamma}_{\mathrm{m}} = v\dot{\lambda}$ and $\dot{\alpha}_b$ are obtained as the solution of the following linear complementary problem:

$$\begin{Bmatrix} \dot{\phi}_{\mathrm{dm}} \\ \dot{\phi}_{\mathrm{s}} \\ \dot{\phi}_{\mathrm{db}} \end{Bmatrix} = \begin{bmatrix} -\dfrac{\gamma_{\mathrm{m}}^2}{c_{\mathrm{mt}}\alpha_{\mathrm{m}}^3} - R'_{\mathrm{m}} & \dfrac{v\gamma_{\mathrm{m}}}{c_{\mathrm{mt}}\alpha_{\mathrm{m}}^2} & 0 \\ \dfrac{v\gamma_{\mathrm{m}}}{c_{\mathrm{mt}}\alpha_{\mathrm{m}}^2} & \dfrac{-1}{c_{\mathrm{mt}}\alpha_{\mathrm{m}}} & 0 \\ 0 & 0 & R'_{\mathrm{b}} \end{bmatrix} \begin{Bmatrix} \dot{\alpha}_{\mathrm{m}} \\ \dot{\lambda} \\ \dot{\alpha}_{\mathrm{b}} \end{Bmatrix} + \begin{Bmatrix} 0 \\ v\dot{\tau} + \mu\dot{\sigma}_2 \\ c_{\mathrm{bn}}\sigma_2\dot{\sigma}_2 + c_{\mathrm{bt}}\tau\dot{\tau} \end{Bmatrix} \leqslant \mathbf{0} \tag{25a}$$

$$\{\dot{\alpha}_{\mathrm{m}} \quad \dot{\lambda} \quad \dot{\alpha}_{\mathrm{b}}\}^{\mathrm{t}} \geqslant \mathbf{0} \tag{25b}$$

$$\{\dot{\phi}_{\mathrm{dm}} \quad \dot{\phi}_{\mathrm{s}} \quad \dot{\phi}_{\mathrm{db}}\}\{\dot{\alpha}_{\mathrm{m}} \quad \dot{\lambda} \quad \dot{\alpha}_{\mathrm{b}}\}^{\mathrm{t}} = \mathbf{0} \tag{25c}$$

The solution of this problem is unique if the principal minors of the matrix in equation (25a) are negative, i.e. if $R'_{\mathrm{m}} > 0$ and $R'_{\mathrm{b}} > 0$. From the first condition in (25a) one may observe that an increment $\dot{\alpha}_{\mathrm{m}} > 0$ is possible only if a sliding $\dot{\lambda} > 0$ takes place; in fact, at the limit state $\phi_{\mathrm{dm}} = 0$ and because of condition (14b) it follows that $\gamma_{\mathrm{m}}^2/c_{\mathrm{mt}}\alpha_{\mathrm{m}}^3 + R'_{\mathrm{m}} > 0 \ \forall\alpha_{\mathrm{m}}$. On the other hand, from the second condition in (25a) it turns out to be possible to get sliding $\dot{\gamma}_{\mathrm{m}} = v\dot{\lambda}$ without damage evolution. Finally, under stress control, the damage evolution in bricks $\dot{\alpha}_{\mathrm{b}}$ turns out to be independent on the mortar joint response ($\dot{\alpha}_{\mathrm{m}}$, $\dot{\lambda}$). In the case $R'_{\mathrm{m}} < 0$ a double solution ($\dot{\alpha}_{\mathrm{m}1} = 0$ and $\dot{\alpha}_{\mathrm{m}2} > 0$) corresponding to a decrement $v\dot{\tau} + \mu\dot{\sigma}_2 < 0$ is obtained. Analogously, if $R'_{\mathrm{b}} < 0$ two solutions ($\dot{\alpha}_{\mathrm{b}1} = 0$ and $\dot{\alpha}_{\mathrm{b}2} > 0$) are obtained corresponding to $c_{\mathrm{bn}}\sigma_2\dot{\sigma}_2 + c_{\mathrm{bt}}\tau\dot{\tau} < 0$. Also, in the case of compressive stress acting on the bed mortar joints, the two solutions correspond to different inelastic strain increments.

It is worth noting that the elements of the matrix in equation (25a) are not determined at the initial undamaged state. However, the evolution from the initial state may be obtained with respect to finite increments by observing that, from condition (22), sliding implies damage evolution. As the sliding intensity can be obtained by posing $\phi_{\mathrm{dm}} = 0$ and noting that $\mathrm{sgn}(\gamma_{\mathrm{m}}) = \mathrm{sgn}(\tau)$, it follows that the sliding is $\gamma_{\mathrm{m}} = \sqrt{2c_{\mathrm{mt}}R_{\mathrm{m}}(\alpha_{\mathrm{m}})}\,\alpha_{\mathrm{m}}\tau/|\tau|$. By setting $\phi_{\mathrm{s}} = 0$ and noting that $|\tau| - \sqrt{2R_{\mathrm{m}}(\alpha_{\mathrm{m}})/c_{\mathrm{mt}}} \geqslant 0$, the limit state condition is obtained:

$$|\tau| + \mu\sigma_2 = \sqrt{2R_{\mathrm{m}}(\alpha_{\mathrm{m}})/c_{\mathrm{mt}}} \tag{26}$$

and this allows the evaluation of the damage induced by the stress components σ_2 and τ. If $|\tau| + \mu\sigma_2 \leqslant 0$, neither sliding nor damage take place, while if $|\tau| + \mu\sigma_2 > 0$ the corresponding damage may be obtained from equation (26).

Since the failure limit states for the mortar joint and the brick are assumed to attain the toughness values R_{mc} and R_{bc}, respectively, for $\alpha_{\mathrm{m}} = 1$ and $\alpha_{\mathrm{b}} = 1$, from equation (26) the limit condition as a function of the applied stresses may be obtained. With reference to proportional loading paths, by substituting the friction $f = -\mu\sigma_2\tau/|\tau|$ in equation (7b) and then in $\phi_{\mathrm{dm}}(\alpha_{\mathrm{m}} = 1) = 0$ the limit state is achieved

$$|\tau| + \mu\sigma_2 = \tau_{\mathrm{mr}} \tag{27}$$

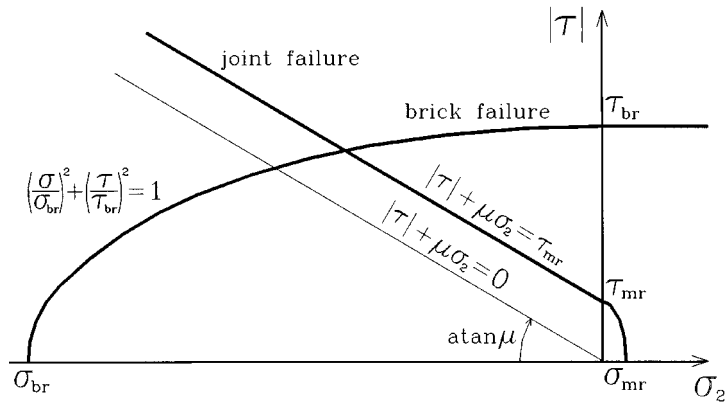

Figure 2. Mortar joint and brick failure domains

The limit state for bricks is obtained by assuming $\phi_{db}(\alpha_b = 1) = 0$ and is given as follows:

$$\sigma_2^2 + \rho_b \tau^2 = \frac{2R_{bc}}{c_{bn}} = \sigma_{br}^2 = \rho_b \tau_{br}^2 \tag{28}$$

where σ_{br} is the masonry compressive strength and $\rho_b = c_{bt}/c_{bn}$. Finally, when $\sigma_2 \leqslant 0$ the following sliding domain is obtained:

$$|\tau| + \mu\sigma_2 = 0 \tag{29}$$

defining the states in which no sliding and damage occur. The limit domains given by equations (20), (21), (27), (28) and (29) are shown in the $(\sigma_2, |\tau|)$ plane in Figure 2.

Good simulations of experimental tests on brick–mortar assemblies have been carried out[1] by assuming the following toughness function:

$$R(\alpha) = \begin{cases} R_c \alpha & 0 < \alpha < 1 \\ R_c \alpha^{-\beta} & \alpha > 1 \end{cases} \tag{30}$$

R_c being the maximum toughness. Moreover, the conditions for the vanishing of the corresponding stress during the damage evolution in the post-peak phase and the irreversibility of the inelastic strains, expressed by equations (14a) and (14b) imply $0 < \beta < 2$. On the other hand, it is worth noting that in the present formulation, the parameters β_m and β_b are intended to characterizing the post-peak responses of the mortar joint and the row of bricks, respectively. Thus, the dependence of the post-peak stress–strain response on the total height of the representative volume element turns out to be automatically taken into account in equation (1) by means of the mortar and brick volume fractions.

Finally, the evaluation of the parameters involved in the proposed model may be carried out through the experimental data provided by the laboratory tests on mortar, brick units and brick–mortar assemblies. To this end, uniaxial tests need to be carried out on bricks (elastic moduli E_b, ν_b and strength τ_{br}), mortar (elastic moduli E_m, ν_m), masonry (compressive strength σ_{br}, failure strain c_{bn} and softening β_b) and on the mortar joint (direct shear strength τ_{mr}, friction coefficient μ, failure shear strain c_{mt}, softening β_m, direct tensile strength σ_{mr}).

3. FINITE ELEMENT ANALYSIS OF BRICK MASONRY SHEAR WALLS

The constitutive model proposed in the previous section has been applied to the analysis of large-scale shear walls having a general shape. To this end, a finite element procedure has been developed based on the plane stress assumption for the wall. Given the complexity of the constitutive equations, finite isoparametric

elements are used. Moreover, since the mortar bed joints are placed in the horizontal plane, quadrilateral finite elements with four nodes have been considered.

It is worth noting that smaller the brick size in comparison to the wall or the pier size the greater is the reliability of the homogenized model. At the limit case of the vanishing size of the brick units the continuum model turns out to be exact and the search for equilibrium states can be carried out through a convergence analysis of finite element models. Yet, in real cases such a situation is not attained and the application of a continuum model to cases in which the brick units have a size which is a relevant portion of the wall size turns out to be approximate whatever the constitutive model considered. Moreover, in the case considered, the constitutive model exhibits a strain softening behaviour that, as is well known, implies strain localization in continuum models, a drawback that may be avoided in the finite element analysis relating the model parameters characterizing the post-critical phase to the finite element size[14] through the definition of a crack band.[15] It must be pointed out that in the case under consideration the crack band thickness is known and corresponds to the bed mortar joint. Thus, even if the non-vanishing brick size involves an approximation, it is possible to define finite elements having a size selected in such a way as to obtain a direct correspondence between a Gauss point and a mortar bed joint. While this consideration allows the definition of a criterion for the selection of the element height, no analogous criterion can be stated in order to define the element width. To this end, the heuristic criterion of relating a Gauss point to a portion of mortar bed joint included between two adjacent mortar head joints has been suggested and checked by a convergence analysis carried out on the examples shown in Section 4.

The non-holonomic character of the constitutive equations proposed in Section 2 implies carrying out the shear walls analysis by means of an incremental procedure based on finite load steps in which load increments or prescribed displacements are applied. Each load step is solved by means of an iterative procedure based on the *initial stress* approach[16] and by assuming the stiffness matrix corresponding to the orthotropic undamaged wall behaviour. The non-linear effects are taken into account in terms of residual forces evaluated once the stress and the internal variables vectors at each Gauss point are updated. To this purpose, the integration algorithm of the constitutive equation in the finite load step described in the appendix has been developed. By distinguishing a load step in which a tensile stress on the bed joint is active ($\sigma_2 > 0$) from those in which a compressive stress ($\sigma_2 \leqslant 0$) is assigned, the algorithm supplies the corresponding increments of the stress and of the internal variables for assigned strain increments, starting from an initial known state.

To get more flexibility in the applications, the algorithm of integration in the finite load step has been implemented in the general purpose code ANSYS.[17] In this way it is possible to carry out three-dimensional analyses of masonry buildings made up of shear walls, to analyse the dynamic response of shear walls to assigned base motions and finally to study the strengthening effects on the structural response provided by reinforcements such as tie rods, etc.

4. EXAMPLES AND SIMULATIONS

4.1. Simulation of rectangular walls

In order to verify the continuum model capabilities in the analysis of brick masonry walls under horizontal actions, the experimental tests by Anthoine *et al.* on two rectangular walls, already simulated by the composite model in the companion paper,[1] have been considered. The dimensions of the walls are 100×135 cm (*low wall*) and 100×200 cm (*high wall*), the wall thickness is 25 cm and they have been subjected to an initial mean compressive stress of 0·6 MPa, due to constant vertical actions at the top and to the wall weight (the masonry mass density is 1750 kg/m^3). The masonry has English bond pattern (see Figure 12 in Reference 1), $5{\cdot}5 \times 12 \times 25$ cm brick unit size and 1 cm mortar joint thickness. Thus, according to the discussion in the previous section, a finite element discretization by rectangular elements of size $14{\cdot}3 \times 13$ cm has been adopted; a sensitivity analysis of the horizontal size of the element has shown a substantial convergence of the results for this choice. The model parameters which have been assumed are shown in Table 1 and have been directly obtained from those of the composite model[1] by means of equations (3)–(6).

The cyclic responses, obtained by imposing horizontal displacements to the top end with restrained rotation, are compared in Figure 3 both with the experimental results and with those provided by the composite model.[1] It may be pointed out that the continuum model, though simpler than the composite one, fairly well simulates the wall strength, the following softening phase, the hysteretic dissipation and the collapse mechanism. However, some differences concerning the rocking mechanism in the high wall are detected during the higher amplitude cycles; an interpretation of this fact will be given by analysing the damage mechanisms.

Figure 4 shows the distributions of the mortar joint damage α_m and of the vertical stress σ_2 in the *low wall* immediately after failure (point A in Figure 3(e)) and at the end of the load history (point C in Figure 3(e)). Already before reaching failure, the mortar joints at the base and the top of the wall undergo opening due to

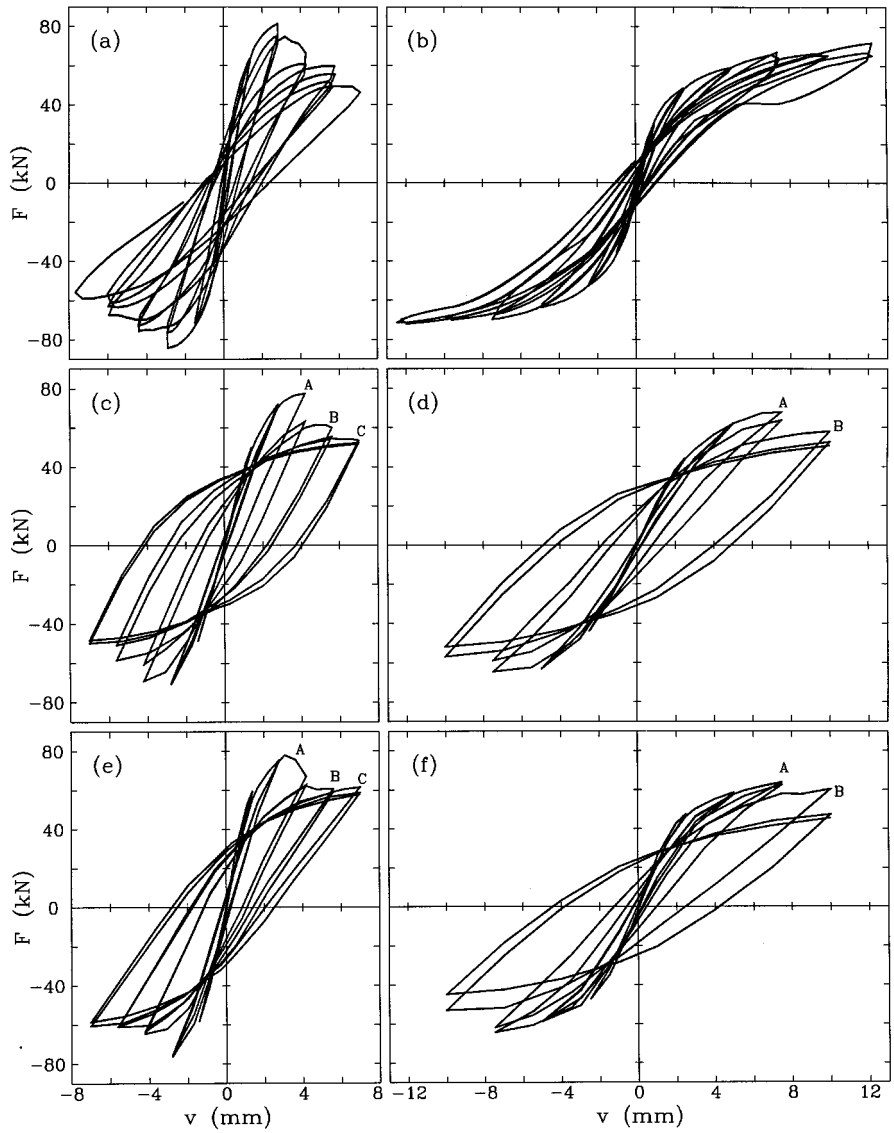

Figure 3. Rectangular masonry panels. Experimental response to horizontal actions:[10] (a) low wall; (b) high wall. Theoretical response by the composite model:[1] (c) low wall; (d) high wall. Theoretical response by the continuum model: (e) low wall; (f) high wall

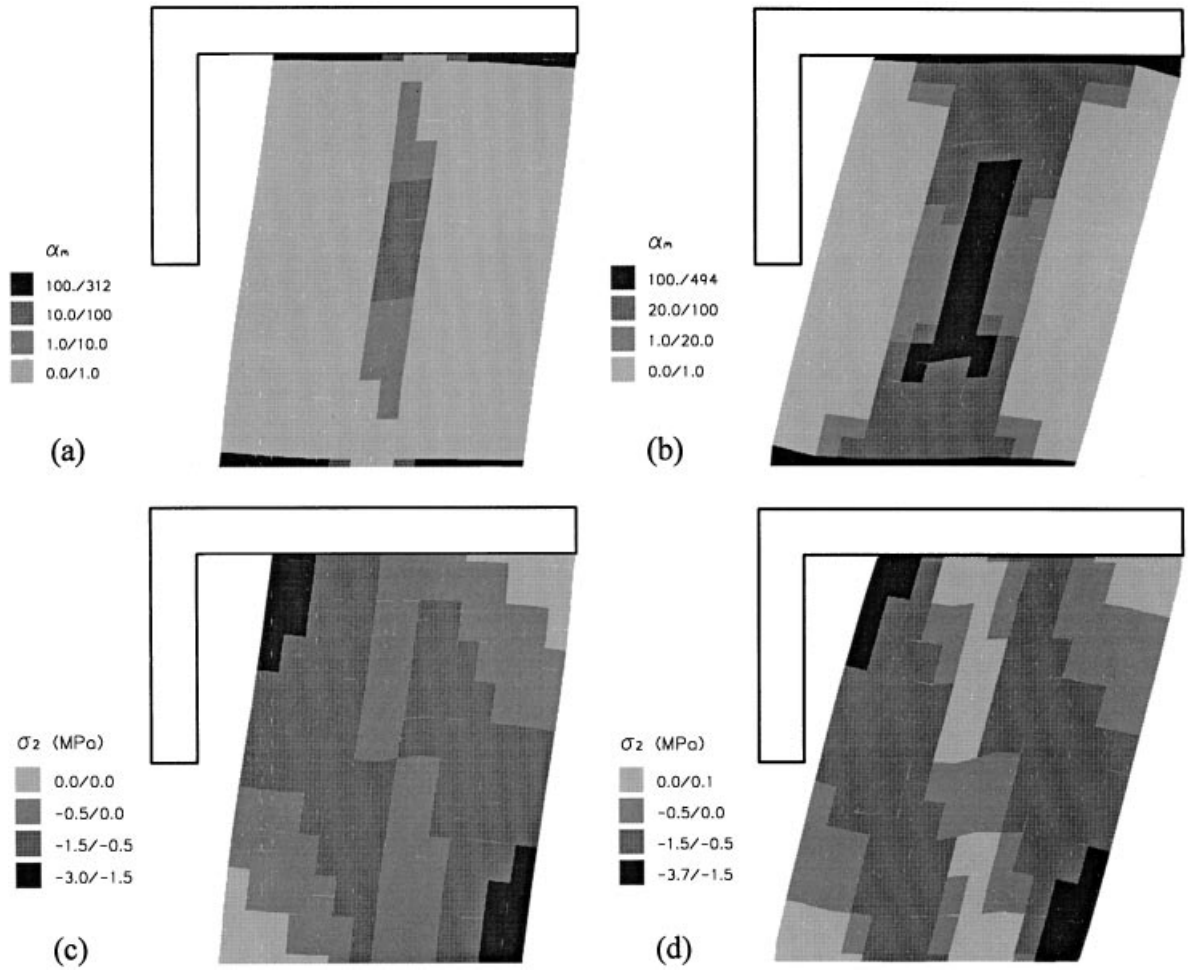

Figure 4. *Low wall.* Mortar joint damage distribution: (a) $v = 3{\cdot}7$ mm; (b) $v = 7$ mm. Vertical stress distribution: (c) $v = 3{\cdot}5$ mm; (d) $v = 7$ mm

Table I. Model parameters assumed in the continuum model

	E_{M1} (MPa)	E_{M2} (MPa)	ν_M	G_M (MPa)	η_m
Elastic moduli	2100	1560	0·194	420	0·154
	σ_{mr} (MPa)	τ_{mr} (MPa)	$1/c_{mt}$ (MPa)	β_m	μ
Mortar joints	0·1	0·4	200	0·8	0·3
	σ_{br} (MPa)	τ_{br} (MPa)	$1/c_{bt}$ (MPa)	β_b	
Brick interface	5	1·2	1000	0·2	

overturning; nevertheless, the limit strength is obtained with the activation in the middle of the wall of sliding damage mechanisms (Figure 4(a)) together with low compressive stress (Figure 4(c)). In the subsequent course of the load history, the damage in the mortar joints of the corners does not grow further, while in the middle of the wall a big area is involved in significant shearing strains and mortar joint damage; such damage

localization reproduces what has been observed both in the experiments[10] and in the composite model. The vertical stress distribution at the end of the load history shows the formation of a slightly inclined central band with tensile stresses, while the overall equilibrium of the wall is guaranteed by two compressed bands. Moreover, the maxima of the compressive stress are attained in the corners and are lower than the compressive strength of the masonry (see Table I), so that a reduced level of damage is obtained in the bricks.

Ignoring the mortar head joint seems not to be very important for the prediction of the post-peak response. As a matter of fact, perceptible openings in the mortar head joints take place only in the wider cycles, so inducing a little reduction on the wall strength (point B and C in Figure 3(c)); on the contrary, Figure 3(e) shows that no reduction of the strength is foreseen by the continuum model from point B to point C. Moreover, the hysteretic dissipation is better simulated by the continuum model with respect to the composite one. In the inclined central band where the tensile stresses act, only detected by the continuum model, no frictional dissipation takes place; the absence of the unloaded band in the composite model may be due to the reduction, induced by the damage in the mortar head joints, of the horizontal tensile stresses.

As for the *high wall* the mortar joint damage and the vertical stress distributions are shown in Figure 5 for two different states in the load history (states A and B in Figure 3(f)). At state A the damage only consists of openings of the corners of the wall due to overturning: the corresponding vertical stress distribution shows a compact domain at the base where low tensile stresses are active and a fairly uniform stress distribution in the middle of the wall. At the end of the load history (state B) a response change is detected, as may be noticed from the increase of dissipation of the last cycle; in fact, sliding mechanisms are activated in a central vertical band (Figure 5(b)) with the consequent formation of two compressed bands and a central one almost unloaded (Figure 5(d)). This result appears to be qualitatively in agreement with that obtained by the composite model; a fair agreement with the experimental results could be acknowledged by observing the presence of small openings of the head mortar joints in the last experimental cycle ($v = 12{\cdot}5$ mm). Also, in the case of the *high wall* the maximum vertical compressive stress is rather low and the brick damage is everywhere negligible with the exception of the wall corners.

It is worth noting that the continuum model seems to simulate the wall response as well as the composite model, which may be considered more detailed. The noticeable saving of computational burden with respect to the composite model gives the opportunity to apply it in the analysis of full scale walls.

4.2. Simulation of a large-scale wall

To evaluate the applicability of the continuum model in analysing full-scale brick masonry walls with openings, a very detailed laboratory test has been considered, concerning the two storey masonry building prototype experimented by Calvi and Magenes[11] at the University of Pavia. The building, having $6 \times 4{\cdot}4$ m plan and 6·4 m height, contains an almost independent shear wall in-plane loaded. The wall here considered is 25 cm thick and has two doors on the first storey and two windows on the second storey; the experimental test has been performed by applying a constant vertical load to the two floors ($P_1 = 14{\cdot}1$ kN, $P_2 = 13{\cdot}8$ kN) followed by a cyclic history in which the imposed displacement at the two floor levels was such that the two corresponding forces were equal.

The finite element model, which is shown in Figure 6, is made up of 1475 nodes and 1330 elements of medium size 19×13 cm. As the lintels are made up by masonry having vertical joints, the continuum model considers a stratified medium with vertical layers. Moreover, a row of elements at the two floor levels has been considered as elastic to simulate the actual stiffness of the experimental set-up. The model parameters, directly obtained by experimental tests on the components (mortar and brick) and their assemblies (triplets, tensile bond strength, masonry prisms),[18] are shown in Table II.

In Figure 7 the experimental and theoretical results are summarized in terms of hysteretic response. By comparing these results, it turns out that the model is able to identify fairly well both the horizontal strength of the wall and its dissipative behaviour. Small differences appear in the first cycles which may be attributed to a non-uniform distribution of the joint strength in the actual wall. In Figure 8 the theoretical results are

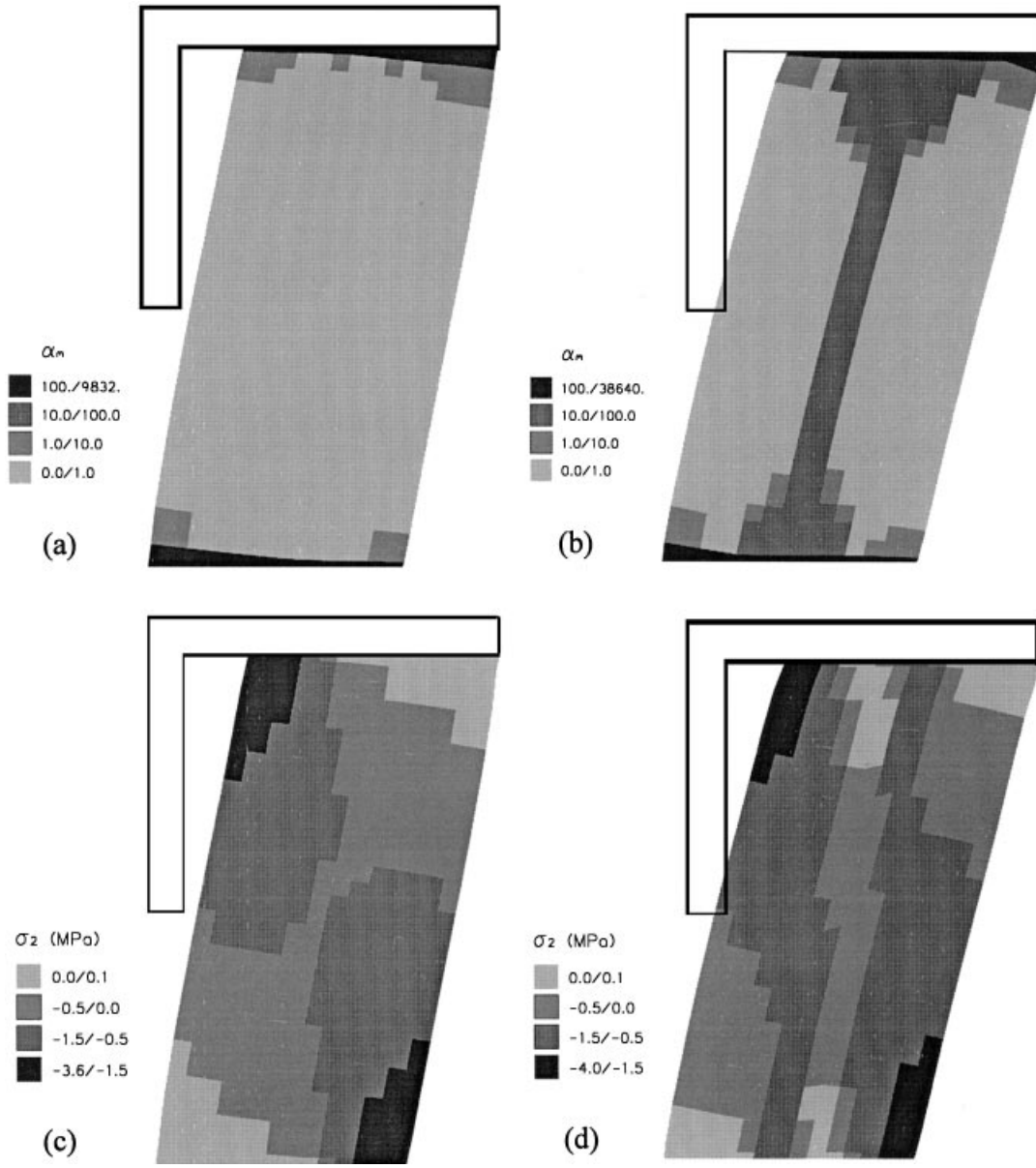

Figure 5. *High wall*. Mortar joint damage distribution: (a) $v = 7{\cdot}5$ mm; (b) $v = 10$ mm. Vertical stress distribution: (c) $v = 7{\cdot}5$ mm; (d) $v = 10$ mm

compared with the experimental ones in terms of the inter-storey response; it turns out that the hysteretic dissipation is mainly located at the first storey, where frictional sliding mechanisms are activated in the joints.

A more detailed description of the evolution of the damage distribution in the mortar joints is given in Figure 9 which shows the mortar joint damage α_m and the vertical stress σ_2 corresponding to two different points of the load history identified in Figures 7 and 8 with A (drift 0·1 per cent) and C (drift 0·3 per cent). The numerical results, which agree fairly well with the experimental ones, showed that during the loading process the first damage appears for drift 0·1 per cent and is localized in the mortar joints in the architrave of the first floor (Figure 9(a)). This is due both to the weakness of the masonry lintels over the doors and to the scanty

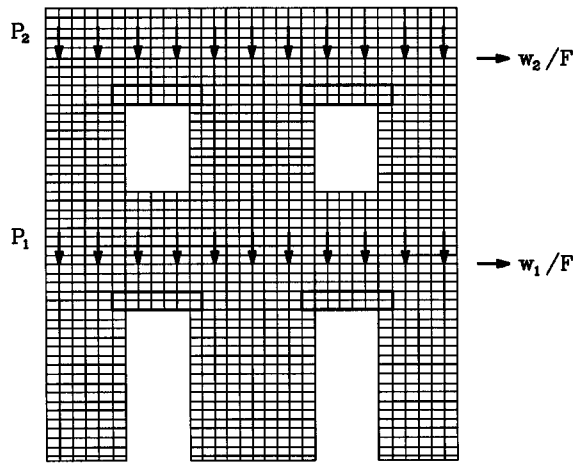

Figure 6. Finite element model of the *door wall*

Table II. Model parameters assumed in the simulation of the large scale wall

	E_{M1} (MPa)	E_{M2} (MPa)	ν_M	G_M (MPa)	η_m
Elastic moduli	1910	1480	0·26	360	0·154
	σ_{mr} (MPa)	τ_{mr} (MPa)	$1/c_{mt}$ (MPa)	β_m	μ
Mortar joints	0·05	0·18	30	0·8	0·577
	σ_{br} (MPa)	τ_{br} (MPa)	$1/c_{bt}$ (MPa)	β_b	
Brick interface	5·9	2	3200	0·4	

contribution of friction to the shear strength, consequent to the low vertical stresses σ_2. For higher horizontal displacements, the base sections of the wall and the central panel also exhibit damage in the mortar joints: in the first case, this is due to the extension and bending of the piers, and in the second case to the shear and bending effect. Increasing the lateral displacement, the damage propagates in the central panel in the form of a Y, as shown in Figure 9(a) for drift of 0·3 per cent.

As shown in Figure 9(b) the vertical stresses are not very high, so that the effects of brick failure are limited and the brick damage distribution is localized to very small areas; it is worth noting that, for drift 0·3 per cent, an inclined unloaded band appears in the central pier, in analogy with the results of the rectangular walls, shown in the previous section (Figure 4(b)). In order to discriminate the opened joints from the damaged ones, the distributions of extension ε_m and sliding γ_m in the joints are shown for drift 0·3 per cent in Figure 10. The extensions (Figure 10(a)) are more significant in the slender lateral piers, which tend to overturn, and in the diagonal of the central pier, together with the sliding (Figure 10(b)); sliding mechanisms are also activated in a vertical central band in the lateral piers, in accordance with the results of the high wall in the previous section (Figure 5(b)). Finally, it has to be observed that a considerable rotation appears at the top of the wall, due to non-uniform compression in the piers as shown in Figure 10, which induces a different kinematic restrain of the top of the piers with respect to the rectangular walls examined in Section 4.1.

4.3. Sensitivity analysis to the model parameters

The proposed FE model sets up an effective support both for the design of experiments and for the following simulation and interpretation of the test results. Moreover, once the validity of the model is

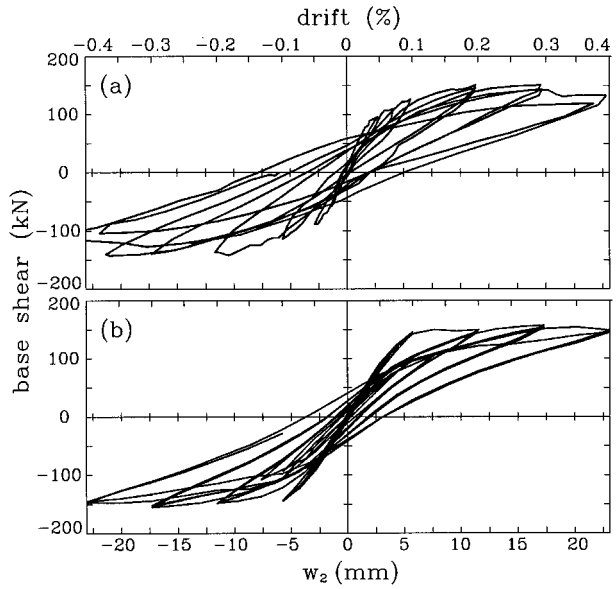

Figure 7. Cyclic response of the *door wall*: (a) experimental; (b) numerical simulation

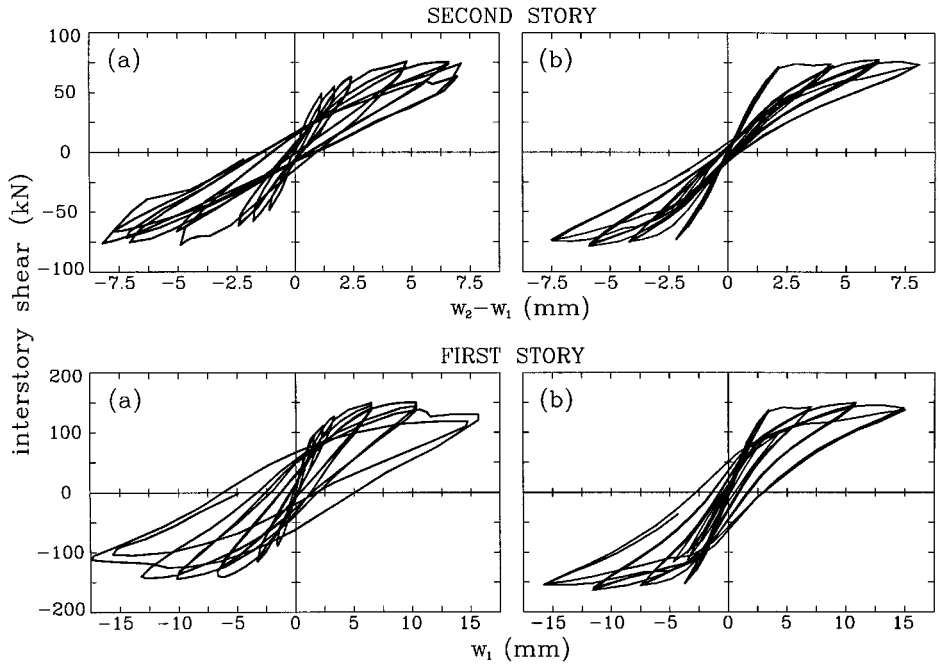

Figure 8. Inter-storey cyclic response: (a) experimental; (b) numerical simulation

ascertained, it may be used as a generator of virtual experiments from which it is possible to understand the role of the wall geometry and the sensitivity to the material data. The model parameters may be collected in three groups, relating to the elastic response, the inelastic response of the mortar joint and the inelastic response of the bricks.

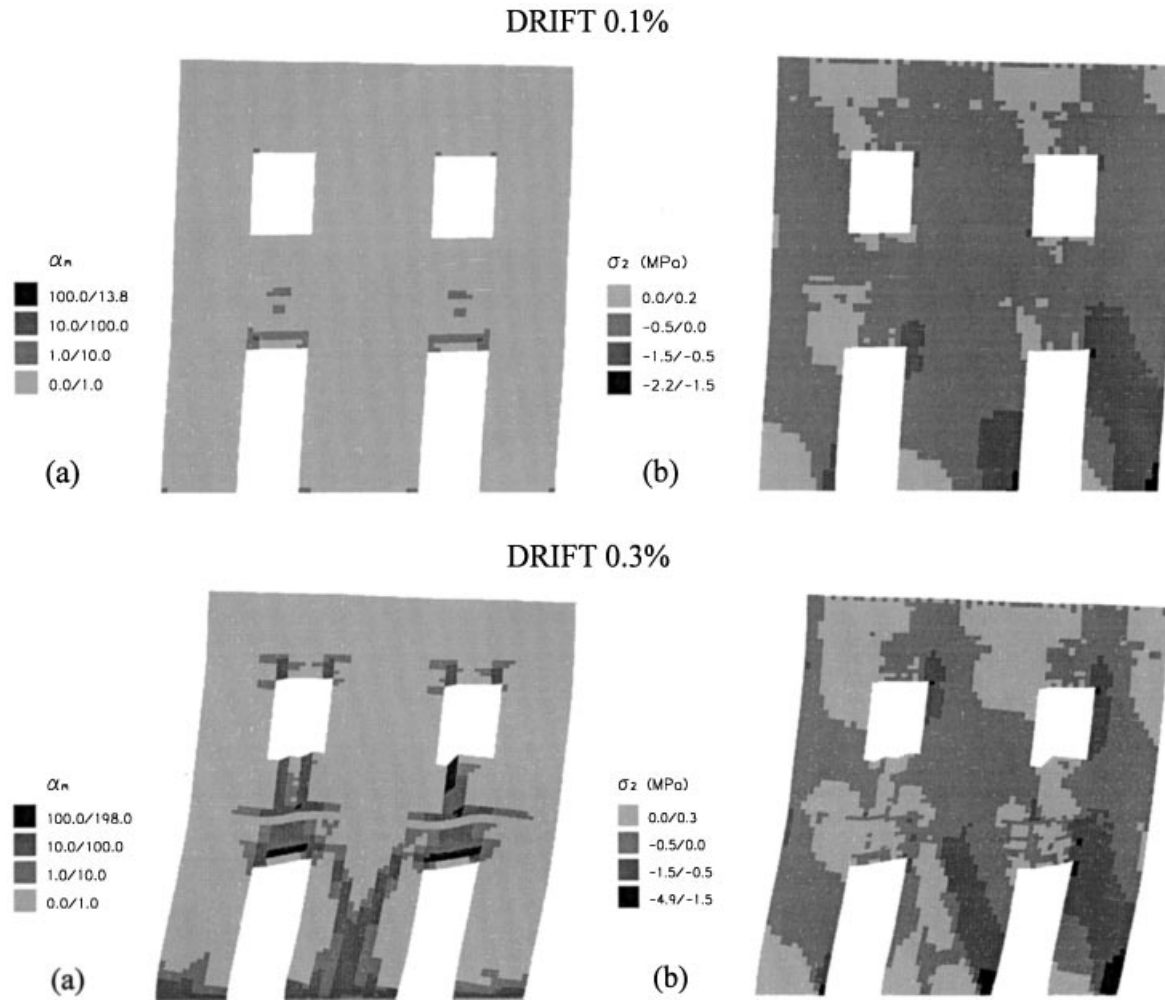

Figure 9. Simulation of experimental tests: (a) mortar joint damage α_m; (b) vertical stress σ_2

The influence of the elastic moduli may be found mostly in the phase that precedes the limit strength of the wall, until the contributions of the inelastic strain are negligible.

Also the model parameters which rule the brick damage are not very significant on the global response in that the initial compressive stresses, due to the dead loads, are usually low and thus the failure of the brick is attained only in very limited zones in the corners of the piers.

In order to understand better the behaviour of brick masonry walls, the sensitivity of the response to the mortar joint model parameters has to be investigated as the more significant damage and failure mechanisms of brick masonry walls under horizontal actions that take place only in the mortar joints. Such parameters are: the friction coefficient μ, the tensile and shear strengths (σ_m,τ_m), the tangential inelastic compliance c_{mt} and the softening parameter β_m.

Considering the friction coefficient a modest influence on the strength may be verified in that, usually, friction sliding takes place in zones where the vertical stress is low, for example in the architraves between the openings and in the unloaded band in the piers. Obviously, a variation of this parameter has an influence on the actions. However, it is difficult to get information of general validity about the sensitivity of this parameter because the wall geometry plays a fundamental role on the activation and interaction among the failure mechanisms.

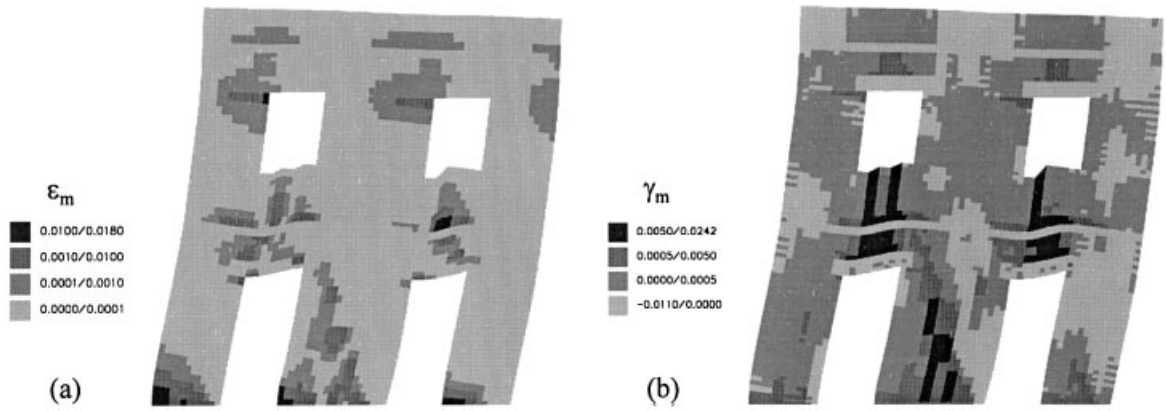

Figure 10. Inelastic deformation in the joints for drift 0·3 percent: (a) extensions ε_m; (b) sliding γ_m

The tensile strength of the joint, which rules the overturning of the piers, has a weak influence also on the global response. In fact overturning is attained only in the slender piers, which are more deformable and give a contribution to the wall strength smaller than that of the squat piers. Moreover, as the tensile strength of the joint is always very low and the joint exhibits a brittle response, it follows that the strength of the slender piers is mainly affected by their shape.

The mortar joint shear strength, which is due to the mortar strength and to the cohesion between mortar and brick, is one of the most variable among the material parameters. In the above-mentioned brick masonry building prototype experimented at the University of Pavia[11] the mortar is poor and this parameter is characterized by a rather low value ($\tau_m = 0{\cdot}18$ MPa). With the aim of understanding the influence of this parameter, the same finite element model has been analysed by adopting a higher value of the mortar joint shear strength ($\tau_m = 1{\cdot}2$ MPa), which can be considered as representative of a cement mortar. The other parameters of the mortar joint have been modified in accordance with previous experimental results on brick-mortar joint specimens ($\sigma_m = 0{\cdot}6$ MPa; $\mu = 0{\cdot}7$; $1/c_{mt} = 520$ MPa). By comparing the hysteretic diagrams of the models (Figure 11) it emerges that, besides a relevant increase of the wall strength (75 per cent), the two walls behave differently: in the case of stronger mortar (Figure 11(b)) the cycles do not exhibit dissipation, with the exception of a low hysteresis for drift 0·4 per cent, and their shape is characteristic of overturning collapse mechanisms. As a matter of fact, Figure 11(c) shows that the mortar joint damage α_m is only located at the base and the top of the three piers of the first storey.

A corroboration of the validity of this theoretical result may be obtained by the comparison with the results of experimental research performed at the University of Illinois at Urbana-Champaign by Abrams and Costley.[19] A small-scale model (1 : 2·5) of the Pavia building prototype with stronger mortar has been tested by a shaking table. The experimental results showed absence of damage in the piers and in the architrave and the activation of the overturning mechanism of the three piers at the first storey. Thus, the results obtained by the numerical model indicate that the differences in the damage distribution are not due to size effects but to the different material properties of the two experimental prototypes.

The influence of the tangential inelastic compliance c_{mt} is analogous to that of the shear strength τ_{mr}, with respect to both the overall response and the damage distribution. This is due to the fact that both parameters determine the value of the failure shearing strain of the mortar–brick joint. Thus, the ability to exhibit relevant deformations without reaching failure, which may be obtained by increasing the shear strength or the inelastic compliance, leads to an increase in overall strength.

Finally, the softening parameter in the joint influences the brittleness of the wall response. However, in full-scale walls with openings, due to the internal static indeterminacy and the non-uniformity of the stress state, a progressive evolution of the damage takes place with the absence of snap-back response.

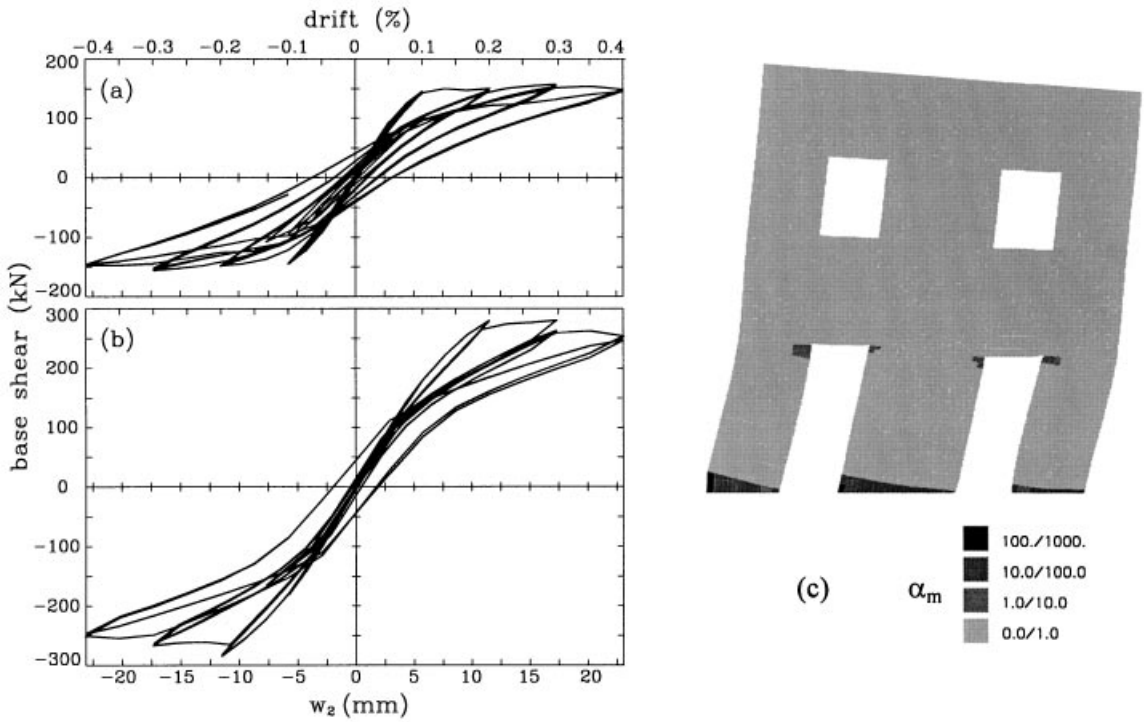

Figure 11. Influence of the mortar joint shear strength: comparison between the Pavia model (a) and the wall with more strength mortar (b); (c) mortar joint damage distribution α_m for drift 0·3 percent in the case of more strength mortar

4.4. Prediction of the seismic response

In the previous section it is shown that the model is able to take in fairly well both the wall strength and, even after the limit strength, the hysteretic response. All of this makes the dynamic analysis meaningful in order to obtain information on the seismic vulnerability of shear walls and thus of unreinforced masonry building. Moreover, the results should give widespread meaning to quasi-static parameters such as strength, ductility and hysteretic damping. In order to get general information about the seismic response of masonry buildings several aspects have to be considered: the geometric and material constants, whose influence may be investigated by the present model through parametric analyses, and the definition of the seismic input, both in term of process length and of frequency content. To this aim, the proposed model may be considered as an effective tool.

As an example, the masonry wall previously described has been subjected to the artificial accelerogram shown in Figure 12(a) applied to the base; its response spectrum (Figure 13(a)) is typical of stiff soils, with a significant frequency content in the range 3–10 Hz, and the intensity corresponds to a peak acceleration $a_{max} = 0{\cdot}35\ g$.

The obtained displacement history of the second floor is shown in figure 12(b), from which it appears that, after the phase of maximum amplitude ($w_2 = 17{\cdot}3$ mm, drift 0·3 per cent), the vibration fades rather quickly, as an effect of the frictional dissipation. Figures 13(b) and 13(c) show the amplification functions of the floor displacements with respect to the base. It emerges that the first natural frequency of the damaged wall is around 3·2 Hz, which is considerably lower than 5·9 Hz, the one obtained by Calvi and Magenes[11] by a series of dynamic identification tests on the undamaged wall, but close to the one obtained after the cyclic static experiment (around 2·9 Hz). The second mode of vibration may be identified by the amplification function of the second floor (8·7 Hz) and probably consists of a vibration of the second storey.

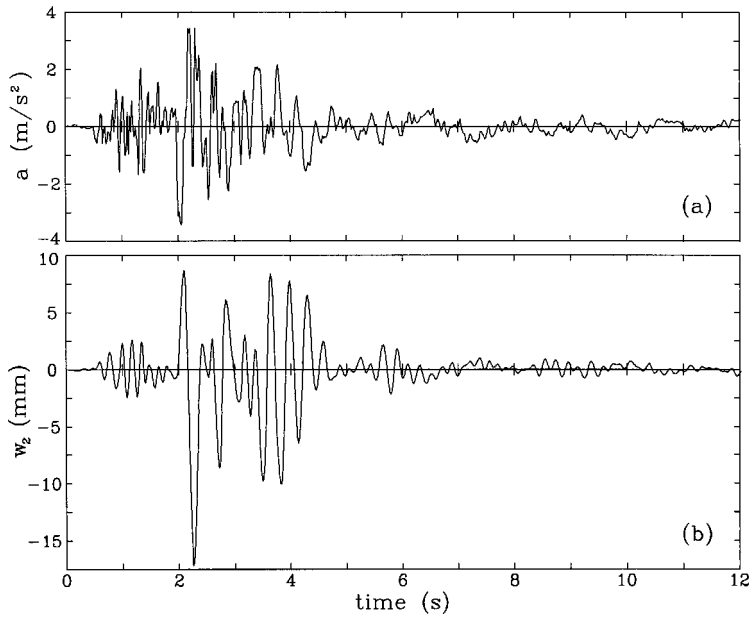

Figure 12. (a) Acceleration time history applied at the base of the wall. (b) Displacement time history on the second floor

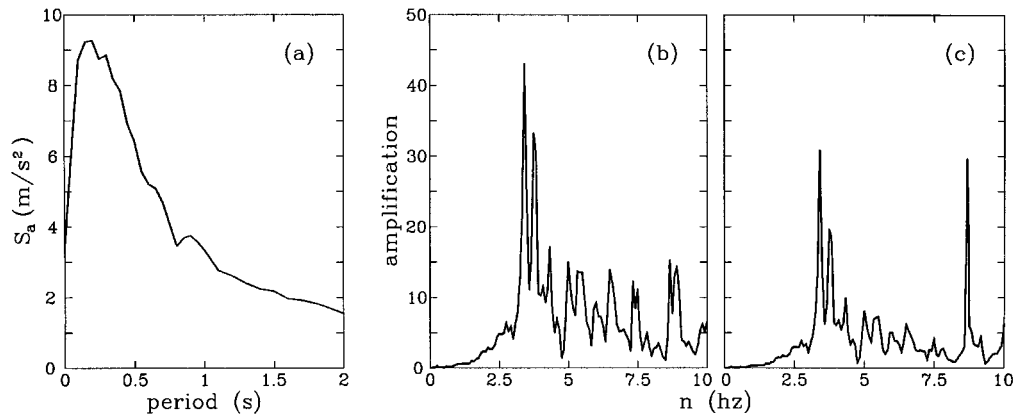

Figure 13. (a) Acceleration response spectrum of the input base motion. Amplification function with respect to the base: (b) first floor displacement, (c) second floor displacement

The diagrams of the floor displacements versus the base shear, shown in Figure 14, look like the ones obtained from the quasi-static analysis (see Figures 7(b) and 14(a)). Finally, Figure 15 shows the distributions of the mortar joint damage and of the vertical stress at the end of the load history. It is worth noting that the mortar joint damage distribution looks similar to the one obtained from the quasi-static excitation (see Figure 9(a), drift 0.3 per cent); this fact gives great importance to the role of cyclic quasi-static experiments on full-scale walls in the evaluation of their seismic vulnerability.

Figure 15(b) shows that in the central pier the vertical stresses, corresponding to the dead loads at the end of the vibrations, are influenced by the damage and the inelastic strains, which induce residual stress concentrations and unloaded zones; on the contrary, in the lateral piers, that overturned during the vibrations, the vertical stress distribution is the same as the initial one.

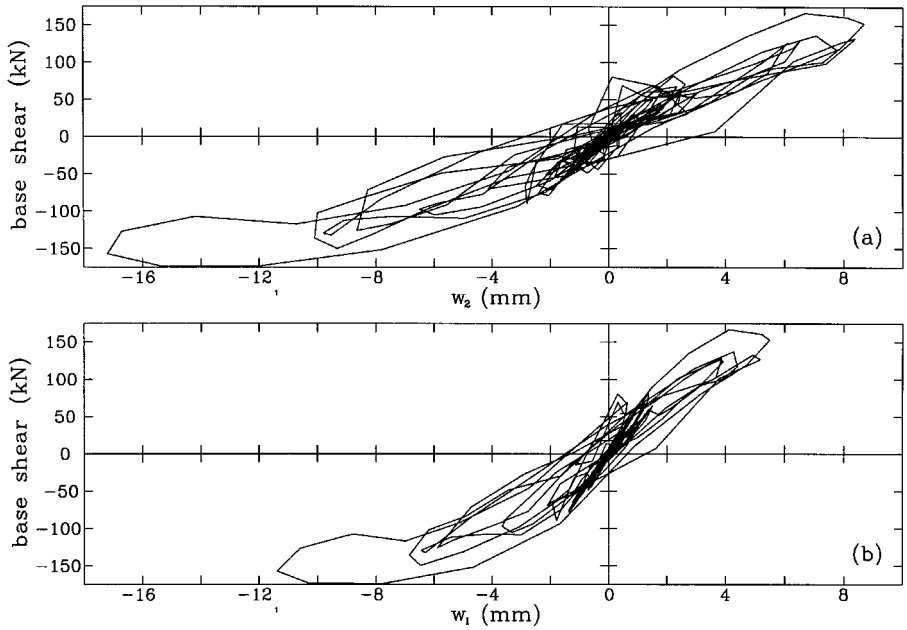

Figure 14. Cyclic response of the large scale wall: (a) second floor; (b) first floor

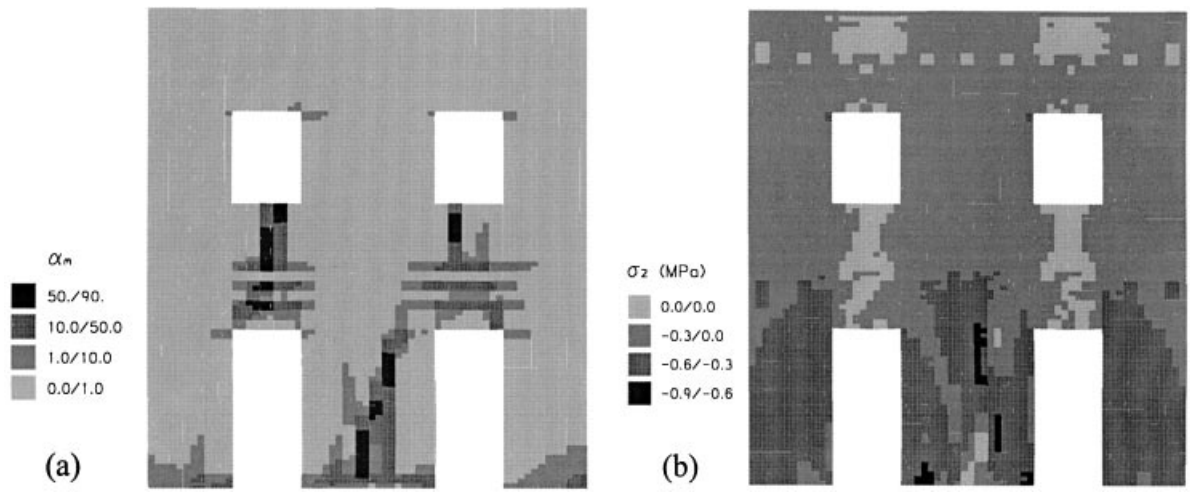

Figure 15. Seismic response of the large-scale wall: (a) mortar joint damage distribution α_m; (b) vertical stress distribution at the end of the earthquake

5. CONCLUSIONS

The mortar joint model proposed in the companion paper[1] has been used to formulate, by means of a homogenization process, a continuum model for brick masonry. Furthermore, the model has been improved by considering the contribution of brick damage, which considers both the strength of the masonry to compressive stresses and the shear strength of bricks.

The model has been implemented in a finite element procedure for the analysis of large-scale brick masonry walls with openings. As, in the model, both damage and friction mechanisms coexist, it is possible to describe the coupling effect of ductility and brittleness which is typical of masonry walls under the horizontal actions representative of the seismic ones.

The finite element procedure requires the definition of the element height in such a way as to obtain a direct correspondence between a Gauss point and a bed mortar joint. In this way the localization effect due to the strain softening behaviour of the damage model is taken into account. This approach turns out to be acceptable if the brick units are small when compared to the wall size which is the more frequent situation in real cases; otherwise, the composite model, proposed in Reference 1, remains the more suitable approach.

A first set of simulations, related to rectangular shear walls, has been devoted to the comparison between the continuum and the composite model; the numerical results show that both models provide a good simulation of the experimental results, thus encouraging the use of the continuum model for its reduction of the computational burdens.

The applicability of the continuum model in analysing actual cases has been ascertained by simulating experimental results on a full-scale two storey masonry building. The numerical results describe fairly well both the cyclic response, in terms of stiffness, strength and dissipative behaviour, and the damage distribution; it is worth noting that the model parameters have been directly obtained by experimental tests on the components (mortar and brick units) and on their assemblies (tensile and shear bond tests, masonry prisms).

The algorithm of integration in the finite load step of the constitutive equation has been implemented in a general purpose finite element code, which makes it possible to perform static and dynamic three-dimensional analyses of masonry buildings.

In order to obtain information on the seismic vulnerability of a masonry building the above-mentioned full-scale wall has been subjected to an artificial accelerogram. The results show that both the cyclic response and the damage distribution look similar to those obtained from the cyclic static analysis, thus corroborating the importance of quasi-static tests.

In the light of these results, the proposed FE model sets up an effective support for the design of experiments and for the following simulation and interpretation; moreover, it may be used as a generator of virtual experiments, from which it is possible to understand the role of the wall geometry and the sensitivity to the material data.

Future applications of this model will be devoted to investigate the influence of the wall geometry and to establish mutual relations between quasi-static parameters such as strength, ductility and hysteretic damping and the actual dynamic response of a masonry wall to seismic actions.

Finally, this model gives the chance to evaluate the effectiveness of some strengthening techniques (such as tie rods, lintels, etc.) in the rehabilitation of the masonry building in historic town centres located in seismic areas.

ACKNOWLEDGEMENTS

The present research was carried out with the financial support of the Italian National Research Council C.N.R.-G.N.D.T.

APPENDIX: INTEGRATION OF THE CONSTITUTIVE EQUATIONS IN THE FINITE LOAD STEP

The integration in the finite load step of the constitutive equations of the continuum model proposed here is a fundamental task in the incremental iterative analysis of masonry walls. Once the state characterized is assumed by given values of the state variables ($\boldsymbol{\varepsilon}$, $\boldsymbol{\sigma}$, ε_m, γ_m, ε_b, γ_b, α_m, α_b) as a reference, the problem concerns variable updating as a consequence of the imposed strain increment $\Delta\boldsymbol{\varepsilon}$. Analogously with the approach considered in the companion paper[1], the condition of compressive or tensile stress acting on the joint plane must be detected; these two events can be distinguished in the finite step by observing from equations (1), (7) and (8) that $\mathrm{sgn}(\sigma_2) = \mathrm{sgn}(\nu_{M12}\varepsilon_1 + \varepsilon_2)$. Thus, on the assumption of proportional increments of the imposed

strain components, the need emerges to select substeps in the loading path, each one encompassing a tensile or compressive stress state on the joint plane.

The case of tensile stress ($\sigma_2 \geqslant 0$) is tackled by considering that, from equations (1), (7) and (8), at the final state:

$$\boldsymbol{\sigma}_f = (\mathbf{K}_M + \eta_m \alpha_{mf} \mathbf{K}_m^* + \eta_b \alpha_{bf} \mathbf{K}_b^{*+})^{-1} \boldsymbol{\varepsilon}_f \tag{31}$$

where $\boldsymbol{\varepsilon}_f = \boldsymbol{\varepsilon} + \Delta\boldsymbol{\varepsilon}$, $\mathbf{K}_m^*$ the mortar joints inelastic compliance matrix (having non-vanishing components $K_{m22}^* = c_{mn}$ and $K_{m33}^* = c_{mt}$), $\mathbf{K}_b^{*+}$ the inelastic compliance matrix of the bricks (having nonvanishing component $K_{b33}^{*+} = c_{bt}$) and $\alpha_{mf} = \alpha_m + \Delta\alpha_m$ and $\alpha_{bf} = \alpha_b + \Delta\alpha_b$ are the final values of the mortar joints and brick damage variables ($\Delta\alpha_m \geqslant 0$, $\Delta\alpha_b \geqslant 0$), respectively.

Having defined $\mathbf{D}_+(\alpha_m, \alpha_b) = (\mathbf{K}_m + \eta_m \alpha_m \mathbf{K}_m^* + \eta_b \alpha_b \mathbf{K}_m^{*+})^{-1}$ and substituting equation (31) in equations (9) and (10) and then in the inequalities (11) and (12), one obtains the set of conditions to be fulfilled simultaneously by the variables α_{mf}, α_{bf} at the final state:

$$\phi_{dm}^+(\boldsymbol{\varepsilon}_f, \alpha_{mf}, \alpha_{bf}) = \tfrac{1}{2} \boldsymbol{\varepsilon}_f^T \mathbf{D}_+(\alpha_{mf}, \alpha_{bf}) \mathbf{K}_m^* \mathbf{D}_+(\alpha_{mf}, \alpha_{bf}) \boldsymbol{\varepsilon}_f - R_m(\alpha_{mf}) \leqslant 0 \tag{32a}$$

$$\phi_{db}^+(\boldsymbol{\varepsilon}_f, \alpha_{mf}, \alpha_{bf}) = \tfrac{1}{2} \boldsymbol{\varepsilon}_f^T \mathbf{D}_+(\alpha_{mf}, \alpha_{bf}) \mathbf{K}_b^{*+} \mathbf{D}_+(\alpha_{mf}, \alpha_{bf}) \boldsymbol{\varepsilon}_f - R_b(\alpha_{bf}) \leqslant 0 \tag{32b}$$

These conditions may be completed with those concerning the irreversibility of the damage and with the complementary nature of limit functions and corresponding damage evolution, so obtaining the following non-linear complementary problem:

$$\phi_{dm}^+(\boldsymbol{\varepsilon}_f, \alpha_m + \Delta\alpha_m, \alpha_b + \Delta\alpha_b) \leqslant 0 \tag{33a}$$

$$\phi_{db}^+(\boldsymbol{\varepsilon}_f, \alpha_m + \Delta\alpha_m, \alpha_b + \Delta\alpha_b) \leqslant 0 \tag{33b}$$

$$\Delta\alpha_m \geqslant 0, \quad \Delta\alpha_b \geqslant 0, \quad \phi_{dm}^+ \Delta\alpha_m = 0, \quad \phi_{db}^+ \Delta\alpha_b = 0 \tag{33c}$$

If $\phi_{dm}^+(\boldsymbol{\varepsilon}_f, \alpha_{mf}, \alpha_{bf}) \leqslant 0$ and $\phi_{db}^+(\boldsymbol{\varepsilon}_f, \alpha_{mf}, \alpha_{bf}) \leqslant 0$, in the load step no damage evolution is detected ($\Delta\alpha_m = 0, \Delta\alpha_b = 0$). Otherwise, the evolution of the damage variables $\Delta\alpha_m$, $\Delta\alpha_b$ may be obtained through an iterative algorithm based on a Newton–Raphson scheme and assuming α_m, α_b as starting values. Once the problem (33) is solved and the damage variables updated, the final stress state is obtained by equation (31).

In the case of compressed joints ($\sigma_2 < 0$), the final stress state may be expressed as follows:

$$\boldsymbol{\sigma}_f = (\mathbf{K}_M + \eta_b \alpha_{bf} \mathbf{K}_b^*)^{-1} (\boldsymbol{\varepsilon}_f - \eta_m \gamma_{mf} \mathbf{e}_3) \tag{34}$$

where $\mathbf{K}_b^*$ is the inelastic compliance matrix of the compressed brick stratum (having non-vanishing components $K_{b22}^* = c_{bn}$ and $K_{b33}^* = c_{bt}$), γ_{mf} is the final unknown value of the friction sliding in the bed joints and $\mathbf{e}_3 = \{0\,0\,1\}^t$. Once defined $\mathbf{D}_-(\alpha_b) = (\mathbf{K}_M + \eta_b \alpha_b \mathbf{K}_b^*)^{-1}$ and substituted equation (34) in conditions (11), (12) and (13), one obtains the set of conditions to be simultaneously fulfilled by the variables α_{mf}, γ_{mf}, α_{bf} at the final state:

$$\phi_{dm}^-(\alpha_{mf}, \gamma_{mf}) = \frac{1}{2} \frac{\gamma_{mf}^2}{c_{mt} \alpha_{mf}^2} - R_m(\alpha_{mf}) \leqslant 0 \tag{35a}$$

$$\phi_{sm}(\boldsymbol{\varepsilon}_f, \alpha_{mf}, \gamma_{mf}, \alpha_{bf}) = \left| \mathbf{e}_3^t \mathbf{D}_-(\alpha_{bf})(\boldsymbol{\varepsilon}_f - \eta_m \gamma_{mf} \mathbf{e}_3) - \frac{\gamma_{mf}}{c_{mt} \alpha_{mf}} \right| + \mu \mathbf{e}_2^t \mathbf{D}_-(\alpha_{bf})(\boldsymbol{\varepsilon}_f - \eta_m \gamma_{mf} \mathbf{e}_3) \leqslant 0 \tag{35b}$$

$$\phi_{db}^-(\boldsymbol{\varepsilon}_f, \gamma_{mf}, \alpha_{bf}) = \tfrac{1}{2} (\boldsymbol{\varepsilon}_f - \eta_m \gamma_{mf} \mathbf{e}_3)^t \mathbf{D}_-(\alpha_{bf}) \mathbf{K}_b^* \mathbf{D}_-(\alpha_{bf})(\boldsymbol{\varepsilon}_f - \eta_m \gamma_{mf} \mathbf{e}_3) - R_b(\alpha_{bf}) \leqslant 0 \tag{35c}$$

being $\mathbf{e}_2 = \{0\,1\,0\}^t$.

Since in finite load steps of moderate amplitude the scalar v is constant (as $v = f/|f|$), it follows by integrating the friction flow rule (14) that $\gamma_{mf} = \gamma_m + v\,\Delta\lambda$ and thus the conditions (35) may be extended in order to obtain the following non-linear complementary problem:

$$\bar{\phi}_{dm}(\alpha_m + \Delta\alpha_m, \gamma_m + v\,\Delta\lambda) \leqslant 0 \tag{36a}$$

$$\phi_{sm}(\boldsymbol{\varepsilon}_f, \alpha_m + \Delta\alpha_m, \gamma_m + v\,\Delta\lambda, \alpha_b + \Delta\alpha_b) \leqslant 0 \tag{36b}$$

$$\bar{\phi}_{db}(\boldsymbol{\varepsilon}_f, \gamma_m + v\,\Delta\lambda, \alpha_b + \Delta\alpha_b) \leqslant 0 \tag{36c}$$

$$\Delta\alpha_m \geqslant 0, \quad \Delta\lambda \geqslant 0, \quad \Delta\alpha_b \geqslant 0 \tag{36d}$$

$$\bar{\phi}_{dm}\Delta\alpha_m = 0, \quad \phi_{sm}\Delta\lambda = 0, \quad \bar{\phi}_{db}\Delta\alpha_b = 0 \tag{36e}$$

Also, in this case the unknowns $\Delta\alpha_m$, $\Delta\lambda$ and $\Delta\alpha_b$ are obtained through an iterative algorithm assuming $\Delta\alpha_m = 0$, $\Delta\alpha_b = 0$ as starting values and based on the Newton–Raphson scheme which is similar to that proposed by Si mo *et al.*[9] Once the internal variables have been updated, the stress state can be evaluated by equation (36).

REFERENCES

1. G. Gambarotta and S. Lagomarsino, 'Damage models for the seismic response of brick masonry shear walls. Part I: The mortar joint model and its applications', *Earthquake eng. struct. dyn.* **26**, 423–439 (1997).
2. H. R. Lofti and P. B. Shing, 'An appraisal of smeared crack models for masonry shear wall analysis', *Comput. struct.* **41**, 413–425 (1991).
3. G. Del Piero, 'Constitutive equation and compatibility of the external loads for linearly elastic masonry-like materials', *Meccanica* **24**, 150–162 (1989).
4. S. Pietruszczak, 'On mechanics of jointed media: Masonry and related problems', in (G. Beer, J. R. Booker and J. P.Carter), (eds), *Computer methods and Advances in Geomechanics*, Vol. 2, pp. 407–415, Balkema, Rotterdam, Brookfield, 1991.
5. S. Pietruszczak and X. Niu, 'A methematical description of macroscopic behaviour of brick masonry', *Int. j. solids struct.* **29**(5), 531–546 (1992).
6. G. Alpa and I. Monetto, 'Microstructural model for dry blok masonry walls with in-plane loading', *J. mech. phys. of solids* **42**, 1159–1175 (1994).
7. G. Maier, A. Nappi and E. Papa, 'Damage models for masonry as a composite materials: a numerical and experimental analysis', in C. S. Desai, E. Krempl, G. Frantziskonis and H. Saadatmanesh, (eds), *Constitutive Laws for Engineering Materials*, pp. 427–432. ASME, New York, 1991.
8. G. N. Pande, J. X. Liang and J. Middleton, 'Equivalent elastic moduli for brick masonry', *Comput. geotechnics* **8**, 243–265 (1989).
9. A. Anthoine, 'Derivation of the in-plane elastic characteristics of masonry through homogenization theory', *Int. j. solids struct.* **32**, 137–163 (1995).
10. A. Anthoine, G. Magonette and G. Magenes, 'Shear-compression testing and analysis of brick masonry walls', in G. Duma (ed.), *Proc. 10th European conference on earthquake engineering*, Vol. 3, pp. 1657–1662, Balkema, Rotterdam, 1995.
11. G. M. Calvi and G. Magenes, 'Experimental research on response of URM building system', in D. P. Abrams and G. M. Calvi (eds), *Proc. U.S.–Italy workshop on guidelines for seismic evaluation and rehabilitation of unreinforced masonry buildings*, State University of New York at Buffalo, NCEER-94-0021, 3-41/57, Pavia, 1994.
12. S. Nemat-Nasser and M. Hori, Micromechanics: Overall Properties of Heterogeneous Materials, Elsevier, Amsterdam, 1993.
13. L. Gambarotta and S. Lagomarsino, 'A microcracked damage model for brittle materials', *Int. j. solids struct.* **30**, 177–198 (1993).
14. S. Pietruszczsaz and Z. Mróz, 'Finite element analysis of deformation of strain softening materials', *Int. j. numer. methods. eng.* **17**, 327–324 (1981).
15. Z. Bazant and L. Cedolin, *Stability of Structures*, Oxford University Press, New York, 1991.
16. O. Zienkiewicz and R. L. Taylor, *The Finite Element Method*, McGraw-Hill, London, 1991.
17. ANSYS User's Manual, Revision 5.0, DN-R300:50, Swanson Analysis Systems, Inc., Houston, PA, 1992.
18. L. Binda, G. Mirabella, C. Tiraboschi and S. Abbaneo, 'Measuring masonry material properties', in D. P. Abrams and G. M. Calvi (eds), *Proc. U.S.–Italy workshop on guidelines for seismic evaluation and rehabilitation of unreinforced masonry buildings*, State University of New York at Buffalo, NCEER-94-0021, 6-3/24, Pavia, 1994.
19. D. P. Abrams and A. C. Costley, 'Dynamic response measurements for URM building systems', in D. P. Abrams and G. M. Calvi (eds), *Proc. U.S.–Italy workshop on guidelines for seismic evaluation and rehabilitation of unreinforced masonry buildings*, State University of New York at Buffalo, NCEER-94-0021, 3-27/39, Pavia, 1994.

